

Breaking the “Redshift Deadlock” - I: Constraining the star formation history of galaxies with sub-millimetre photometric redshifts

D.H. Hughes¹, I. Arétxaga¹, E.L. Chapin¹, E. Gaztañaga¹, J.S. Dunlop², M.J. Devlin³, M. Halpern⁴, J. Gundersen⁵, J. Klein³, C.B. Netterfield⁶, L. Olmi⁷, D. Scott⁸, G. Tucker⁹

¹ Instituto Nacional de Astrofísica, Óptica y Electrónica (INAOE), Aptdo. Postal 51 y 216, Puebla, Mexico

² Institute for Astronomy, Univ. of Edinburgh, Blackford Hill, Edinburgh, EH9 3HJ, UK

³ Dept. of Physics & Astronomy, Univ. of Pennsylvania, 209 South 33rd St., Philadelphia PA 19104-6396, USA

⁴ Dept. of Physics & Astronomy, Univ. of British Columbia, 6224 Agricultural Road, Vancouver, B.C. V6T 1Z1, Canada

⁵ Dept. of Physics, Univ. of Miami, 1320 Campo Sano Drive, Coral Gables, FL 33146, USA

⁶ Dept. of Astronomy, Univ. of Toronto, 60 St. George St., Toronto, Ontario, MSS 1A1, Canada

⁷ Dept. of Physics & Astronomy, Univ. of Massachusetts, Amherst, MA 01003, USA

⁸ Dept. of Physics & Astronomy, Univ. of British Columbia, 2219 Main Mall, Vancouver, B.C. V6T 1Z4, Canada

⁹ Dept. of Physics, Box 1843, Brown Univ., Providence, RI 02912-1843, USA

7 February 2020

ABSTRACT

Future extragalactic sub-millimetre and millimetre surveys have the potential to provide a sensitive census of the level of obscured star formation in galaxies at all redshifts. While in general there is good agreement between the source counts from existing SCUBA (850 μ m) and MAMBO (1.25 mm) surveys of different depths and areas, it remains difficult to determine the redshift distribution and bolometric luminosities of the sub-millimetre and millimetre galaxy population. This is principally due to the ambiguity in identifying an individual sub-millimetre source with its optical, IR or radio counterpart which, in turn, prevents a confident measurement of the spectroscopic redshift. Additionally, the lack of data measuring the rest-frame FIR spectral peak of the sub-millimetre galaxies gives rise to poor constraints on their rest-frame FIR luminosities and star formation rates. In this paper we describe simulations that demonstrate how photometric redshifts derived from future sub-millimetre experiments, in particular the Balloon-borne Large Aperture Submillimetre Telescope and the Herschel satellite, can constrain the global star formation rates for luminous galaxies ($L_{\text{FIR}} > 3 \times 10^{12} L_{\odot}$) with an accuracy of $\sim 20\%$ at redshifts $0.5 < z < 5.5$.

Key words: submillimetre, millimetre, cosmology, galaxy evolution, star-formation

1 INTRODUCTION

The star-formation history of the high- z starburst galaxy population can be determined from an accurate measurement of the integral sub-millimetre (sub-mm) and millimetre (mm) source-counts, and the luminosity and redshift distributions of sub-mm and mm-selected galaxies. The contribution of these sources to the total FIR-mm background, measured by COBE (Puget et al. 1996; Hauser et al. 1998; Fixsen et al. 1998), places an additional strong constraint on the acceptable evolutionary models. A series of cosmological sub-mm surveys, that cover a sufficiently wide range of complementary depths, areas, and wavelengths are able to

discriminate between competing models of massive galaxy formation. The evolution of the luminosity function and clustering of sources in these surveys will reveal whether galaxies form via the classical picture of early monolithic collapse at high redshifts, or via gradual merging of halos at lower redshifts (Kauffmann et al. 1993; Baugh, Cole & Frenck 1996; Somerville et al. 2001).

It is now generally accepted that the luminosity density, due to star formation activity in galaxies, is roughly constant between $z \sim 1 - 4$. A series of ground-based sub-mm 850 μ m surveys (Smail et al. 1997; Hughes et al. 1998; Barger et al. 1998; Eales et al. 1999; Eales et al. 2000; Scott et al. 2001; Fox et al. 2001; Borys et al. 2001), undertaken with

the SCUBA camera (Holland et al. 1999) on the 15-m James Clerk Maxwell Telescope (JCMT), have contributed significantly to this understanding. Prior to the first SCUBA results, the optical surveys suggested (contrastingly) that the density of star-formation declined by a factor of ~ 5 over the same redshift range (Steidel et al. 1996; Madau et al. 1996). This discrepancy has highlighted the importance of including a correction for dust extinction in the optical-UV estimates of star formation rates. Nevertheless, the contribution of optically-selected starburst galaxies to the sub-mm background still remains uncertain (Chapman et al. 2000; Peacock et al. 2000).

One important caveat to this opening statement is the fact that we actually have no accurate information on the redshift distribution of the sub-mm galaxy population. There are ~ 100 galaxies identified in $850\mu\text{m}$ surveys at a level > 2 mJy. The lack of confident optical, or IR identifications (*e.g.* Hughes et al. 1998; Richards 1999), and thus precise redshifts for the sub-mm galaxies, was a source for the early scepticism of the claims that there existed no evidence for a decline in density of star formation at $z > 2$.

The use of the radio–sub-mm ($850\mu\text{m}/1.4\text{GHz}$) spectral index has gained popularity as a valuable diagnostic of redshift (Hughes et al. 1998; Carilli & Yun 1999; Carilli & Yun 2000; Smail et al. 2000; Barger, Cowie & Richards 2000). The follow-up of SCUBA surveys, and more recently 1.2mm MAMBO surveys (Bertoldi et al. 2000), with VLA 1.4 GHz observations has become the commonly accepted method to measure the redshift distribution of sub-mm galaxies. However this technique requires extremely sensitive radio observations. For example, in order that a radio survey detects $> 80\%$ of bright sub-mm galaxies ($S_{850\mu\text{m}} > 6$ mJy) at $z > 1.5$, then a $3\sigma \leq 6\mu\text{Jy}$ survey must be conducted at 1.4 GHz (Aretxaga et al. 2001b). The necessity of such an ultra-deep radio survey prohibits this technique from being applied to the wider-area ($\simeq 1$ sq. deg.) sub-mm surveys proposed for the next few years. An alternative, and more reliable method exists: namely the use of sub-mm–FIR photometric redshifts, provided that one can control the accuracy of the experimental data. In general, ground-based sub-mm observations with the Caltech Submillimetre Observatory (CSO) and JCMT at 350 and $450\mu\text{m}$ respectively have lacked a combination of sufficient calibration accuracy and sensitivity to offer useful constraints. Similar problems have afflicted the FIR ($90\text{--}170\mu\text{m}$) observations with the Infrared Space Observatory (ISO). It should be noted that regardless of these difficulties, it has been possible to statistically associate a faint population of sub-mm sources (~ 3 mJy at $850\mu\text{m}$) with FIR galaxies detected at $170\mu\text{m}$ in the deep ISO FIRBACK survey (Scott et al. 2000).

It is well known that cosmological studies at sub-mm and mm wavelengths ($\lambda > 850\mu\text{m}$) benefit greatly from a strong negative k-correction. This effect is due to the steep spectral index of the optically-thin Rayleigh-Jeans emission from dust grains radiating at 30–70 K in star formation regions. Consequently a starburst galaxy of fixed luminosity will have a similar flux density between $z = 1 - 8$ (Blain & Longair 1993). Shorter wavelength sub-mm – FIR observations ($\lambda > 200\mu\text{m}$) benefit to a lesser extent, unless a trend of increasing dust temperature with increasing luminosity (or redshift) is taken into account (Fig. 1). At mm wavelengths, sources actually become brighter with increas-

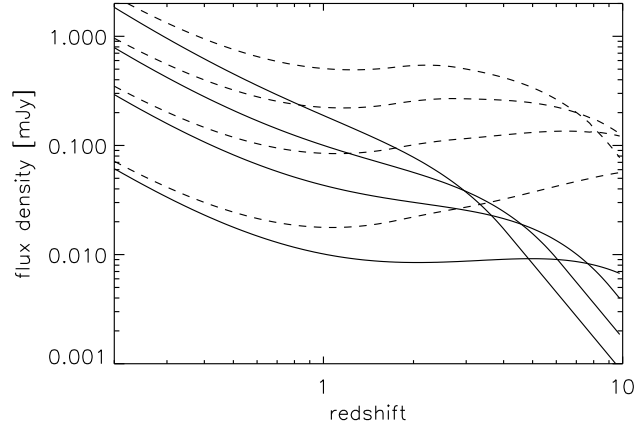


Figure 1. Flux density vs. redshift for a galaxy with a FIR luminosity similar to M82, $L_{\text{FIR}} \sim 3 \times 10^{10} L_{\odot}$. Solid curves, in order of decreasing flux density at $z = 0.1$, represent models at 250, 350, 500 and $850\mu\text{m}$ assuming the following cosmological model: $\Omega_M = 0.3, \Omega_{\Lambda} = 0.7, H_0 = 67\text{km s}^{-1}\text{Mpc}^{-1}$. The dashed curves illustrate the effect of luminosity evolution (following the model described in §2.2), which manifests itself as a factor of 2 increase in dust temperature (from 45 K to 90K) between $z = 0$ and $z = 2.2$.

ing redshift. The 50-m Large Millimetre Telescope (LMT), currently under construction at 4500 m on Volcán Sierra Negra in Mexico, will soon exploit this advantage.

In this paper (Paper I) we summarise a new balloon-borne experiment, *BLAST* (Devlin et al. 2001), that will conduct sensitive, simultaneous sub-mm surveys at 250, 350 and $500\mu\text{m}$ with a calibration accuracy of 5%. We describe the simulations that have guided the design of the future *BLAST* surveys, and demonstrate how the rest-frame FIR–sub-mm SEDs of galaxies can be used to measure their photometric redshifts with a typical 1σ accuracy of $\Delta z \sim \pm 0.6$. Thus we can break the current *redshift deadlock* that limits our understanding of the evolution of the sub-mm galaxy population. From such precision in the individual galaxy redshifts, we can determine the star formation history for luminous sub-mm galaxies brighter than $3 \times 10^{12} L_{\odot}$ with an accuracy of $\sim 20\%$. Furthermore we illustrate how these estimates can be improved with sub-mm observations using the more sensitive SPIRE camera on the Herschel satellite (formerly FIRST), and additionally with the inclusion of longer-wavelength ground-based data. In the second paper of this series (Aretxaga et al. 2001b, Paper II) we apply this same technique to the existing multi-frequency data for the population of sub-mm galaxies detected in SCUBA and MAMBO surveys. We include, for the first time, an appropriate treatment of the observational errors at sub-mm to radio wavelengths, and provide an accurate measurement of the redshift distribution for sub-mm galaxies. In the third paper of this series (Gaztañaga et al. 2002, Paper III) we address clustering issues using sub-mm photometric redshifts.

1.1 Status of Sub-millimetre and Millimetre Surveys

The possibility of conducting cosmological surveys at sub-mm and mm wavelengths has been realised in the last few

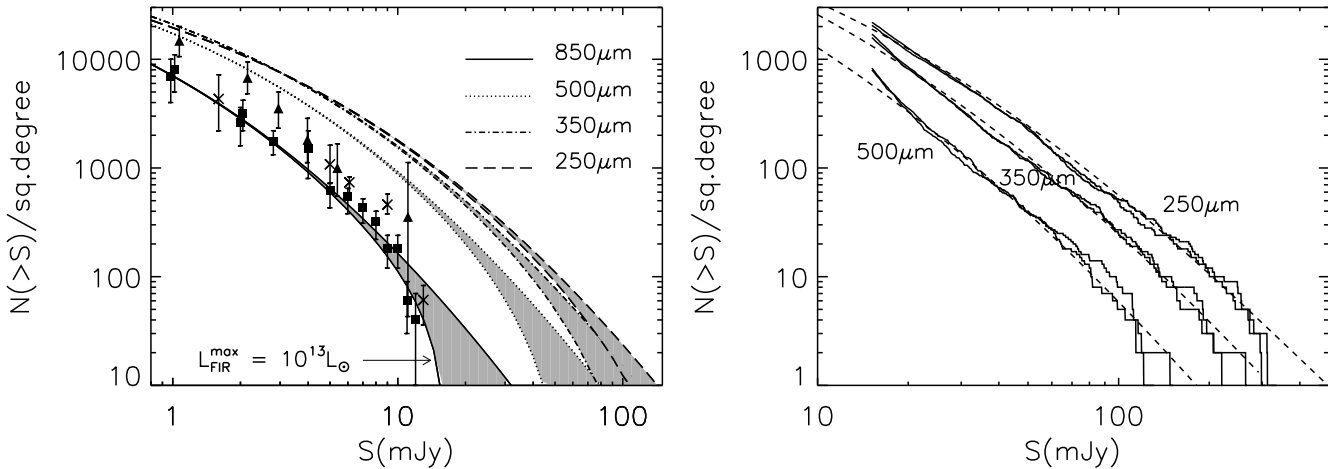


Figure 2. Integrated source-counts at sub-mm wavelengths for a model in which the IRAS 60 μ m luminosity function is evolved as $(1+z)^{3.2}$ upto $z=2$, and maintained constant (with no further evolution) for $2 < z < 6$. The SED of Arp220 is adopted to represent the whole galaxy population. *Left panel:* The curves represent the predicted source-counts at 850, 500, 350 and 250 μ m. The measured source-counts from SCUBA surveys at 850 μ m (Scott et al. 2001, and references therein) are shown as filled squares. Additional 850 μ m source-counts from Borys et al. (2001) are shown as solid triangles. The flux-densities of the MAMBO 1.25 mm source-counts are scaled upwards by a factor of 2.25 to represent the equivalent measurements at 850 μ m, assuming the MAMBO sources lie at redshifts $1 < z < 6$, and are shown as crosses (Bertoldi et al. 2000). The models also show the effect of a high-luminosity cut-off (at $L_{\text{FIR}} > 10^{13} L_{\odot}$) in the sub-mm population. The shaded areas illustrate the regions of parameter space that need to be searched with future experiments to improve our understanding of the evolution of the luminous high- z sub-mm galaxies. *Right panel:* Integrated source-counts for extragalactic *BLAST* surveys at 250, 350 and 500 μ m. The dashed-lines show the same evolutionary model described for the left-panel. The histograms illustrate the extracted source-counts at each wavelength from two different Monte-Carlo simulations of 1 sq.deg surveys that use a library of 13 SEDs. These simulations explore evolutionary models with small differences in the strength of evolution and the redshift distribution of sources. The details of the Monte-Carlo simulations are summarised here (§2.2) and elsewhere (Aretxaga et al. 2001a)

years with the development and successful commissioning of sensitive bolometer arrays, *e.g.* SCUBA (Holland et al. 1999), SHARC (Hunter, Benford, Serabyn 1996), MAMBO (Kreysa et al. 1998), BOLOCAM (Glenn et al. 1998), all of which will be upgraded within the next few years.

The existing 850 μ m SCUBA and 1.25 mm MAMBO surveys are limited in their ability to constrain the evolutionary models of the sub-mm galaxy population. The practical reasons for these limitations have been described elsewhere (Hughes 2000) and can be summarised as follows: restricted wavelength coverage (enforced by the limited number of FIR-mm atmospheric windows available to ground-based observatories); low spatial resolution (resulting in both a high extragalactic confusion limit and poor positional accuracy); restricted field-of-view with the current sub-mm and mm bolometer arrays (typically 5 sq. arcmin); and low system sensitivity (a combination of instrument noise, size of telescope aperture and telescope surface accuracy, sky transmission and sky noise) which restrict even the widest and shallowest sub-mm surveys to areas < 0.3 sq.deg (Scott et al. 2001; Fox et al. 2001). In the effort to obtain these wide-area shallow surveys, the current sub-mm and mm observations are necessarily only sensitive to the most luminous star-forming galaxies ($L_{\text{FIR}} > 10^{12} L_{\odot}$, or $\text{SFR} > 100 M_{\odot} \text{yr}^{-1}$) assuming the population is dominated by galaxies at redshifts > 1 .

These initial SCUBA and MAMBO observations have demonstrated the necessity for larger-area surveys, and also shorter-wavelength (250–500 μ m) sub-mm observations.

Partial solutions on the short time-scale (within the next 3 years) to the above limitations can be found in two new large-aperture, single-dish, ground-based, millimetre-wavelength telescopes: the 100-m Green Bank Telescope (GBT) which has recently been commissioned, and the LMT which will *see* first-light in late 2003. Both telescopes will provide significantly greater mm-wavelength survey sensitivities than the current confusion-limited data. Also the development of new large-format filled-array cameras, SCUBA-II for the JCMT, and SHARC-II for the CSO, will dramatically enhance the efficiency of conducting ground-based 850 μ m and 350 μ m sub-mm surveys respectively. In addition, large sub-mm interferometers, which are also under construction (*e.g.* SMA) will soon provide accurate positions for a limited number of the brightest sub-mm sources.

Despite these new ground-based facilities, there will still remain large uncertainties in the redshifts and rest-frame FIR luminosities for the majority of sub-mm galaxies, and thus an inaccurate constraint on the star formation history of the entire sub-mm population.

Once it begins operation beyond 2008 on a high-altitude, dry Chilean site, ALMA will undoubtedly solve many of these difficulties with its powerful combination of receivers operating between 350 μ m and 3 mm, and high (sub-arcsec) spatial resolution. The expected launch of the Herschel satellite in 2008 will also bring the chance to map large areas of the extragalactic sky at 250–500 μ m with high sensitivity. However, before 2008, long-duration (~ 15 day) balloon-borne experiments, *e.g.* *BLAST* – Balloon-

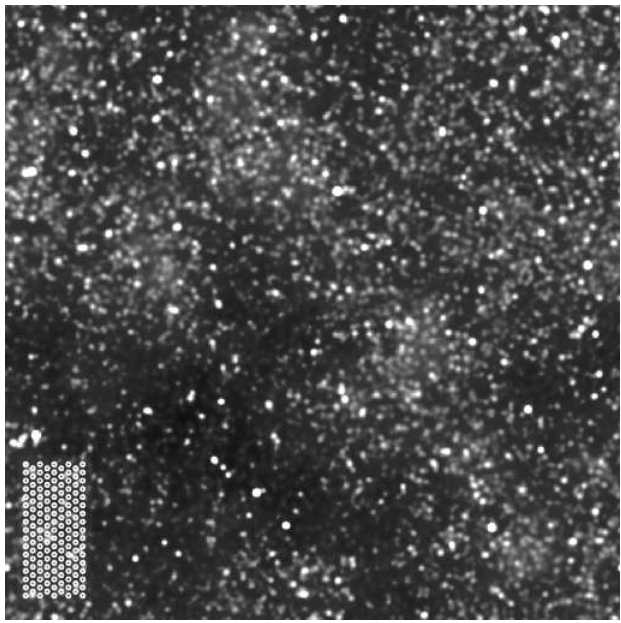


Figure 3. A simulated confusion-limited *BLAST* 250 μm survey with a FWHM resolution of 30 arcsec and 1σ sensitivity of 5 mJy. The evolutionary history for this sub-mm population is described in §2.2. The assumptions regarding the clustering of sub-mm galaxies are described elsewhere (Hughes & Gaztañaga 2000, Gaztañaga & Hughes 2001). The simulation includes a foreground component of Galactic cirrus ($I_{250\mu\text{m}} = 2.6 \text{ MJy/sr}$) and covers an area of 1 sq. deg. The instantaneous field-of-view (85 sq. arcmins) of the *BLAST* array at 250 μm is shown in the lower-left corner. This single 50-hour *BLAST* survey, and other wider-area, shallower surveys are summarised in Table 1.

borne Large-Aperture Sub-millimetre Telescope (Devlin et al. 2001), will conduct sub-mm surveys with significantly greater sensitivity than is available from even the largest ground-based sub-mm observatories.

Hereafter, for the sake of brevity, sub-mm and mm wavelengths will be referred to as *sub-mm* unless explicitly stated otherwise, and a *sub-mm galaxy* is considered to be an optically-obscured starburst galaxy detected in a blank-field SCUBA or MAMBO survey. The following cosmological model is adopted throughout the paper: $\Omega_\Lambda = 0.7$, $\Omega_M = 0.3$, $H_0 = 67 \text{ km s}^{-1} \text{ Mpc}^{-1}$.

1.2 Ambiguities in the Counterparts of Sub-mm Galaxies

The current 850 μm SCUBA and 1.25 mm MAMBO surveys (with 15 and 11 arcsec FWHM resolution respectively) are struggling to identify the sub-mm sources with their optical, IR and radio counterparts. Hence, the redshift distribution and luminosities of the sub-mm sources are still uncertain. This results directly from the sub-mm positional errors of $\sim 2 - 3$ arcsec that are typical for even the highest S/N sub-mm detections, and to a lesser extent from the lack of data measuring the redshifted FIR spectral peak at 200–450 μm .

The positions of the brightest sub-mm sources ($S_{850\mu\text{m}} > 8 \text{ mJy}$) which, with some exceptions, are detected

in the widest, shallowest SCUBA surveys (Scott et al. 2001; Eales et al. 2000), can be improved with follow-up mm-interferometric observations (Frayer et al. 1998; Gear et al. 2000; Lutz et al. 2001). However ambiguous optical identifications, and hence uncertain redshifts still remain, even with ≤ 2 arcsec resolution and sub-arcsec positional errors (e.g. Downes et al. 1999). It should be no surprise that sub-mm selected galaxies, including those with mm-interferometric detections, do not always have optical counterparts, since high- z galaxies observed in the earliest stages of formation may be heavily obscured by dust. Indeed, this is the most compelling reason for conducting the sub-mm surveys in the first instance, and therefore searches for the counterparts are expected to be more successful at longer IR wavelengths. A powerful demonstration of the importance of IR imaging has been presented by Lutz et al. (2001) who found a faint IR source ($K = 21.4$), with no optical counterpart ($I > 27.5$), associated with the improved mm-interferometric position of the brightest sub-mm source detected in the SCUBA survey of the Lockman Hole (Scott et al. 2001). Earlier examples by Smail et al. (1999) and Frayer et al. (2000) also reveal high-redshift, $z > 2$, IR galaxies, with no optical or radio counterparts, within 2–3 arcsec of two lensed SCUBA sources (Smail et al. 1997). The original optical counterparts of these SCUBA sources were identified as bright low-redshift ($z \sim 0.5$) galaxies 5–10 arcsec distant from the sub-mm sources (Smail et al. 1998). The natural consequence of these mis-identifications is an inaccurate determination of redshift distribution and star-formation history of high- z galaxies.

1.3 Uncertainties in the SEDs and Redshifts of Sub-mm Galaxies

There are a few cases of spectroscopically-determined redshifts for sub-mm galaxies associated with AGN (Frayer et al. 1998; Ivison et al. 2000). In almost all cases these galaxies have been identified in sub-mm surveys of lensing clusters (Smail et al. 1997; Smail et al. 2000; Knudsen et al. 2001). Their optical spectroscopic redshifts are consistent with the overall redshift distribution, which places the population of sub-mm galaxies between $z = 1 - 4$. The evidence for this redshift distribution of sub-mm galaxies is based on simple comparisons of their IR-radio spectral energy distributions (SEDs), usually one or two detections plus a few limits, with some template, often the ultra-luminous IR galaxy (ULIRG) Arp220 (Hughes et al. 1998; Smail et al. 1999; Barger, Cowie & Richards 2000; Bertoldi et al. 2000).

This raises an obvious question: *What classes of local galaxies offer the most useful analogues of the high- z sub-mm population?* In order to address this question we must measure the full rest-frame X-ray to radio SEDs of individual high- z sub-mm galaxies, measure the dispersion in the shapes of their SEDs and their range of luminosities (which may depend on redshift), and thus determine the accuracy with which the SEDs of high- z sub-mm galaxies can be characterised by a limited number of local template galaxies.

As mentioned previously, optical and IR follow-up observations of those few SCUBA sources for which unambiguous identifications exist have revealed that the sub-mm counterparts are often optically-obscured, extremely red objects (EROs) with $I - K > 6$ (Smail et al. 1999; Gear et

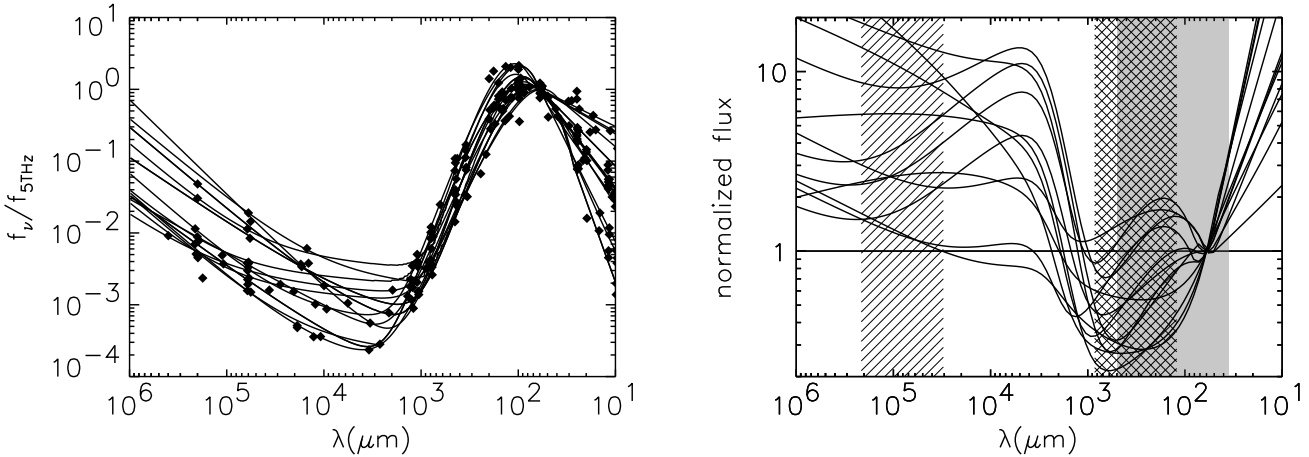


Figure 4. *Left panel:* Rest-frame spectral energy distributions (SEDs) of 13 starburst galaxies, ULIRGs and AGN, normalized at $60\mu\text{m}$. Lines represent the best fit SED models to the data (diamonds) and include contributions from non-thermal synchrotron emission, free-free and grey-body thermal emission. The parameters that describe the composite model for each galaxy, previously unpublished SED data and references for the remaining SED data are given in Aretxaga et al. (2001b); *Right panel:* Composite SED models for the identical 13 template galaxies shown in the left panel, normalized at $60\mu\text{m}$ and scaled to the flux density of Arp220 at each wavelength. The vertically bounded-regions (slanted, crossed and shaded) correspond to the rest-frame wavelength regimes covered by observations at 1.4 GHz, $850\mu\text{m}$ and in the *BLAST* filters (500 – $250\mu\text{m}$) respectively for galaxies at $z = 0$ – 6 . This representation of the SEDs shows more clearly the wavelength regimes in which the minimum dispersion in galaxy colours can be expected. Hence photometric redshifts determined from flux ratios between ~ 100 – $1000\mu\text{m}$ are the most independent of assumptions regarding the SED of the sub-mm galaxy.

al. 2000; Lutz et al. 2001), although in a few cases the sub-mm counterparts are blue galaxies, with weak AGN (e.g. SMM02399–0136, Ivison et al. 2001). Also the evidence indicating that SCUBA galaxies are forming stars at a very high-rate ($> 100M_{\odot}/\text{yr}$) implies that local dusty ULIRGs may also be suitable analogues of high- z sub-mm sources. Unfortunately the SEDs of this local class of luminous star-forming galaxies vary significantly with increasing FIR luminosity (Sanders & Mirabel 1996). Furthermore, there are few starburst galaxies at $z > 1$ for which complete IR–radio SEDs exist.

Despite the diversity in the properties of sub-mm galaxies (Ivison et al. 2000), efforts have been made to place them in the context of an evolutionary model of galaxy formation. Thus, in order to make some progress on describing the redshift distribution of the high- z sub-mm galaxy population, it has been necessary to compare their SEDs with those of local and distant starburst galaxies and radio-quiet AGN.

In an early SCUBA $850\mu\text{m}$ survey of the northern Hubble Deep Field (Hughes et al. 1998), the SEDs of Arp220 and Mrk231 were adopted as templates from which redshifted colours could be calculated under different cosmologies. This choice was justified since their SEDs, when normalised at $850\mu\text{m}$, bound those of the majority of other ULIRGs, radio-quiet quasars, Seyfert galaxies with circum-nuclear starforming rings, and starburst galaxies. It was on the strength of their colours between 15 , 170 , 450 , $850\mu\text{m}$ and 1.4 GHz that the HDF-N sub-mm galaxies were placed at redshifts $0.9 < z < 3.8$.

Similar subsequent investigations have also used the sub-mm–radio colours to measure photometric redshifts (Lilly et al. 1999; Carilli & Yun 1999; Barger, Cowie & Richards 2000; Carilli & Yun 2000; Smail et al. 2000) and

have concluded that galaxies selected from MAMBO and SCUBA surveys have median redshifts of $z = 2.5$ and $z = 1.9$, respectively. In summary, the consensus is that the population of sub-mm galaxies is distributed between redshifts $z = 1$ – 4 , yet the details of this distribution are unknown. It is common to describe the redshift of individual galaxies as “*in the range of, with a best guess of*”.

This ambiguity in the optical, IR and radio identifications of sub-mm galaxies, and the lack of precision in their redshift distribution, motivated a successful NASA proposal to build and fly *BLAST*, a Balloon-borne Large-Aperture Sub-millimetre Telescope (Devlin et al. 2001). *BLAST* has a 2-m primary aperture and is equipped with large-format bolometer cameras operating at 250 , 350 and $500\mu\text{m}$ which are prototypes of the SPIRE focal-plane cameras for the Herschel satellite. *BLAST* is scheduled for a test-flight in November 2002. During a series of long-duration (~ 15 day) balloon flights in Antarctica from 2003 onwards, *BLAST* will conduct large-area sub-mm surveys (Table 1), and will provide sensitive rest-frame FIR–sub-mm data for > 5000 galaxies. In the remainder of this paper we describe how the rest-frame FIR–sub-mm colours of individual galaxies can constrain their photometric redshifts, and hence the luminosities and SFRs of the sub-mm galaxy population.

2 PHOTOMETRIC REDSHIFTS FROM WIDE-AREA SUB-MILLIMETRE SURVEYS

2.1 Designing the Sub-mm Surveys

Realistic galaxy survey simulations, which incorporate evolutionary models that are consistent with the observed sub-mm and mm source-counts (Fig.2) have been developed to

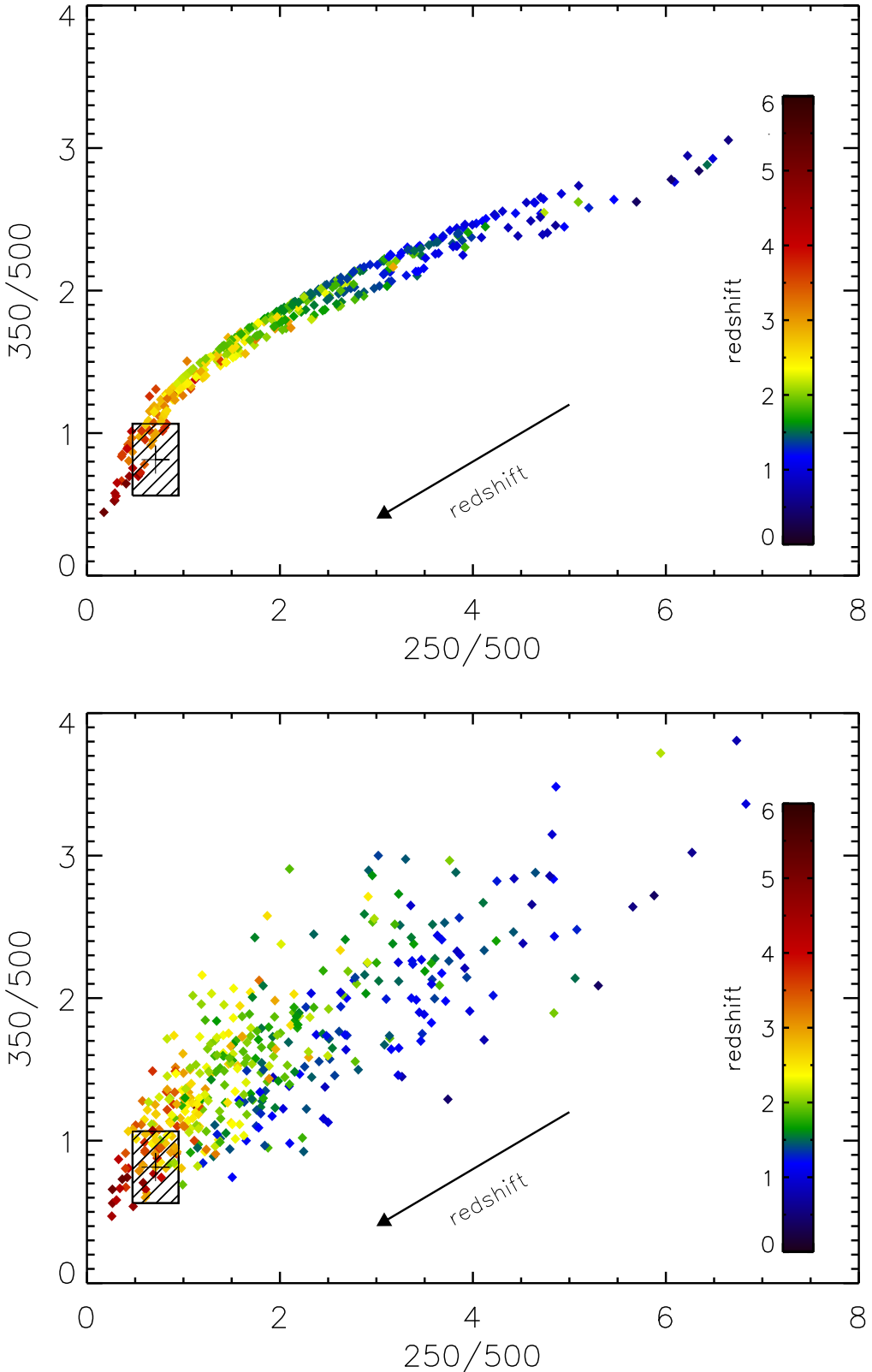


Figure 5. Colour-colour ($350\mu\text{m}/500\mu\text{m}$ vs. $250\mu\text{m}/500\mu\text{m}$) vs. redshift distribution for 424 galaxies detected ($> 3\sigma$) simultaneously by *BLAST* in all 3 filters in a simulated 1 sq. deg survey. *Top Panel*: Colour distribution of detected galaxies without the inclusion of observational (photometric or calibration) errors. *Bottom Panel*: Colour distribution of detected galaxies with the inclusion of observational errors (5% absolute calibration and a random measurement error drawn from a $1\sigma = 5\text{ mJy}$ distribution), which dominate the scatter. The black cross marks the position of a $4 \times 10^{12} L_\odot$ galaxy at $z = 2.81$. The hashed rectangle represents the 1σ error on the measured colours. The redshift probability distribution for this galaxy is shown in Fig.6.

assist in the design of these future balloon-borne sub-mm experiments (Hughes & Gaztañaga 2000; Gaztañaga & Hughes 2001; Chapin et al. 2001). These simulations also include a Galactic cirrus component, generated by extrapolating the measured FIR cirrus power-spectrum determined from IRAS and ISO observations to the higher spatial-frequencies of the *BLAST* observations, and by extrapolating the $100\mu\text{m}$ surface brightness ($I_{100\mu\text{m}}$) to the longer *BLAST* wavelengths assuming a temperature of 18K and grain emissivity index $\beta = 2$ (Désert et al. 1990; Gautier et al. 1992; Lagache & Puget 2000). The combined galaxy and cirrus simulations (Fig.3), which produce artificial multi-wavelength images at different spatial resolutions, address real issues confronting existing current and forthcoming surveys. For example, they describe how the measured source-counts can be affected by telescope resolution, extragalactic and Galactic source-confusion, survey sensitivity and noise, and sampling variances due to clustering and shot-noise.

The discrepancy shown in Fig.2 between the bright-end source-counts in the $850\mu\text{m}$ SCUBA and 1.25 mm MAMBO surveys (Eales et al. 2000; Bertoldi et al. 2000; Scott et al. 2001; Borys et al. 2001), and a visual inspection of their reconstructed maps, suggests that the clustering of sub-mm galaxies may be influencing the statistics (Gaztañaga & Hughes 2001). Taken at face value, the steepening of the $850\mu\text{m}$ counts for sources > 10 mJy can be interpreted as evidence for an under-density of galaxies in the survey-field providing those particular data (due to cosmic variance), or perhaps a high-luminosity cut-off in the luminosity function for galaxies $> 10^{13}L_\odot$ (Fig.2). A plausible alternative explanation is simply the fact that, with so few bright sources detected (5–10 galaxies in 0.1 sq. degs), the counts in this regime are extremely sensitive to differences between the SEDs of the most luminous sub-mm galaxies. Only sensitive wider-area (≥ 0.5 sq. deg.), rest-frame FIR surveys (similar to those to be conducted by *BLAST* or Herschel) can distinguish between these possible alternatives.

Simulations of future *BLAST* observations have guided the choice of survey areas, with the intention of avoiding any artifacts in the final data due to galaxy clustering. The same simulations have also guided the choice of survey depths to ensure that the deepest *BLAST* surveys reach below the extragalactic confusion-limit.

In the absence of any foreground cirrus, the simulation indicates that the extragalactic 3σ confusion limit of *BLAST* at $250\text{--}500\mu\text{m}$ will be $\sim 20 - 30$ mJy. For comparison the traditional estimate of extragalactic confusion, 1 source/30 beams (Condon 1974), suggests that confusion will begin to dominate below 30 mJy. We demand that extragalactic sources dominate the total confusion noise, $\sigma_c(\text{galaxies}) + \sigma_c(\text{cirrus})$, in the *BLAST* survey fields. Thus we impose the criteria that $\sigma_c(\text{galaxies}) > 5 - 10\sigma_c(\text{cirrus})$ at $250\mu\text{m}$. Different realisations of Galactic cirrus (by varying the SED, surface brightness, and structure function of the dust distribution) were added as a foreground component to our sub-mm galaxy simulations. An analysis of the accuracy with which it is possible to extract the model sub-mm extragalactic source-counts, in the presence of Galactic cirrus at the *BLAST* wavelengths and at these spatial resolutions, places a limit of $I_{100\mu\text{m}} < 1.4 \text{ MJy/sr}$ on the maximum $100\mu\text{m}$ surface brightness of the Galactic foreground emission. The most recent all-sky cirrus maps (Schlegel et al.

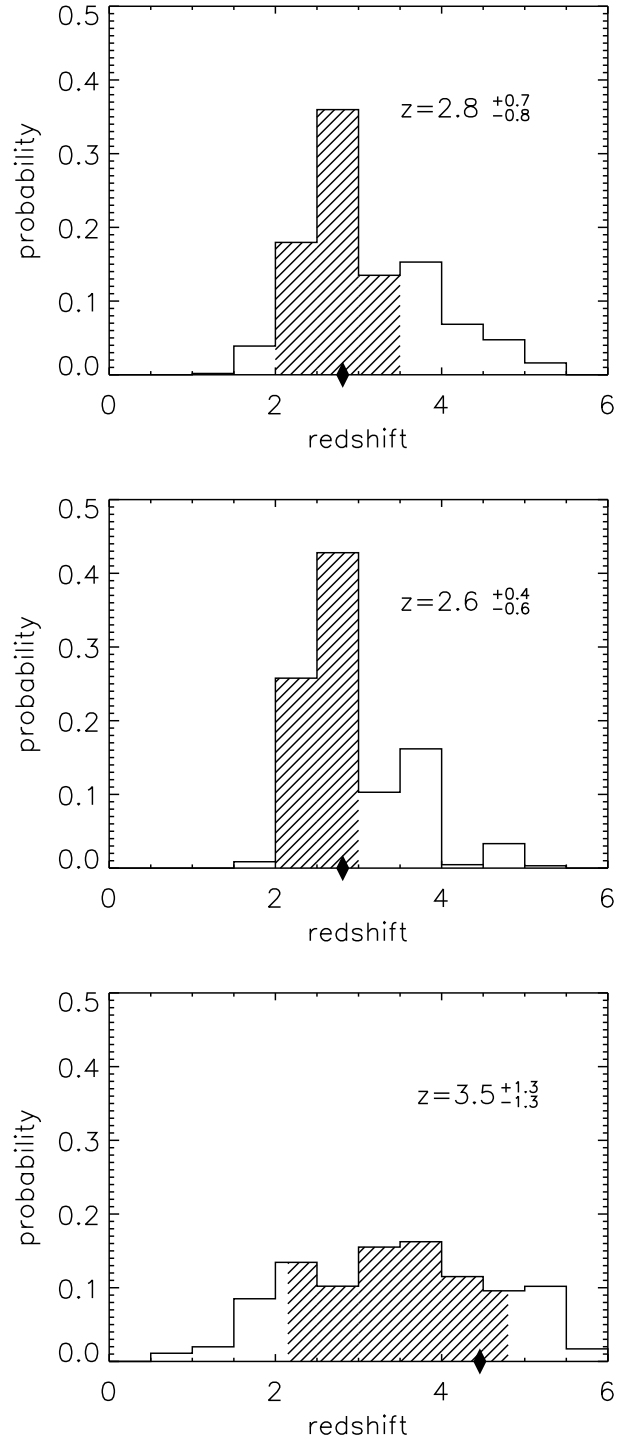


Figure 6. Redshift probability distributions for a selection of galaxies detected by *BLAST*. In all panels the diamonds mark the true redshifts of the galaxies. The photometric redshifts (modes and 68% confidence intervals) are indicated in the labels and represented as the shaded areas of the histograms. *Top panel*: $4 \times 10^{12}L_\odot$ galaxy at $z = 2.81$, detected at $250\mu\text{m}$ (19 mJy), $350\mu\text{m}$ (21 mJy) and $500\mu\text{m}$ (26 mJy), slightly below the *BLAST* survey confusion limit. The colours of this galaxy are represented as a cross in Fig.5. *Middle panel*: $6 \times 10^{12}L_\odot$ galaxy at $z = 2.81$, detected at $250\mu\text{m}$ (34 mJy), $350\mu\text{m}$ (56 mJy) and $500\mu\text{m}$ (45 mJy) with high S/N, above the *BLAST* survey confusion limit. *Bottom panel*: $4 \times 10^{12}L_\odot$ galaxy at $z = 4.46$, detected only at $500\mu\text{m}$ (22 mJy).

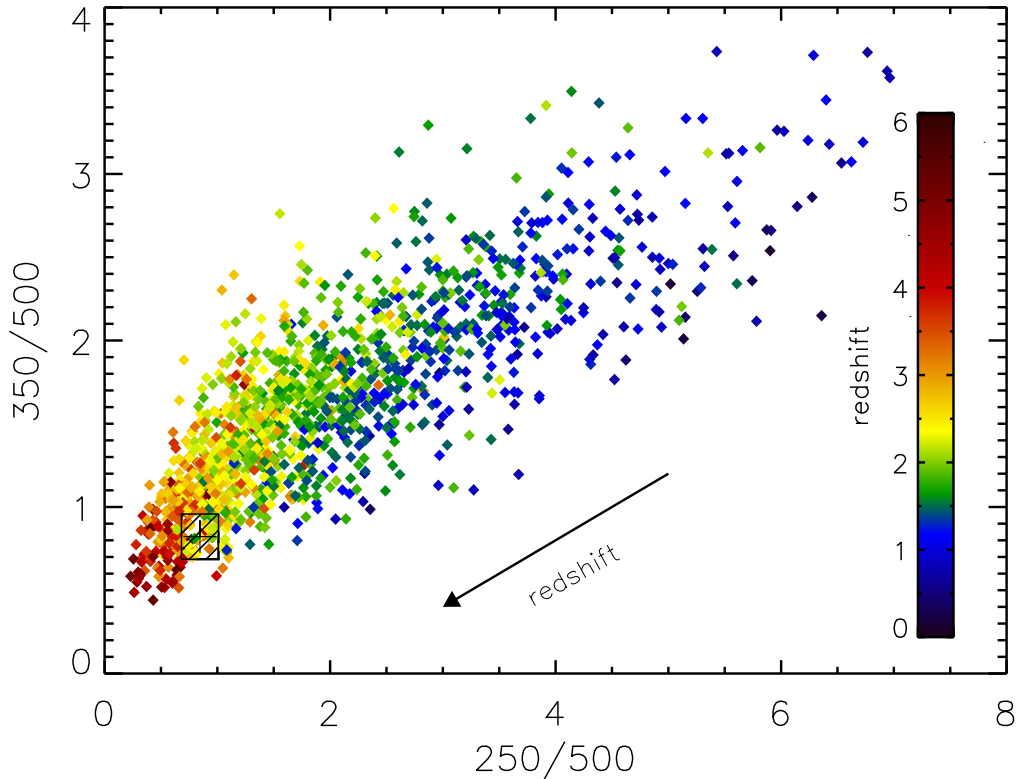


Figure 7. Monte-Carlo simulations of the colour-colour ($350\mu\text{m}/500\mu\text{m}$ vs. $250\mu\text{m}/500\mu\text{m}$) vs. redshift distribution for 1380 galaxies detected simultaneously by SPIRE at 250, 350 and $500\mu\text{m}$ with observational errors (5% absolute calibration and a random measurement error of 2.5 mJy) in a 1 sq. deg survey. The black cross and hashed rectangle marks the colours for the identical $4 \times 10^{12} L_\odot$ galaxy at $z = 2.81$ shown in Figs. 5 and 6.

1998) show that this requirement restricts *BLAST* surveys to $\sim 19\%$ of the sky available to our Antarctica flights (at a latitude of $\sim -78^\circ$), a fact that must be taken into account when planning the large-area surveys. This is an important consideration for those surveys which require complementary longer-wavelength ground-based data to provide discriminatory power in determining redshifts at $z > 4$ (§2.3). Simulations to determine the accuracy of the source-extraction suggest that, under these cirrus conditions, we are still able to recover 70% of the sources with $250\text{--}500\mu\text{m}$ fluxes between 15 mJy and the nominal confusion limit.

The final requirement of our planned *BLAST* surveys is that a sufficient area is surveyed to reduce the clustering noise to the level of $\sim 3\%$ in the $250\text{--}500\mu\text{m}$ counts. The predictions of Gaztañaga & Hughes (2001) suggest a minimum *BLAST* survey area of 1.0 sq. deg is necessary.

Hence, during a single long-duration balloon flight from Antarctica, *BLAST* will conduct a series of simultaneous large-area surveys (1–36 sq. deg.) at 250, 350 and $500\mu\text{m}$, down to a 1σ sensitivity of 5 mJy, detecting in each survey ~ 1000 luminous sub-mm galaxies ($> 10^{12} L_\odot$) between $0.5 < z < 6$ (Table 1). The accuracy with which redshifts can be determined from these observations is discussed in the following sections.

2.2 Monte-Carlo Simulations of Sub-mm Galaxy Colours

Measurements of photometric redshifts determined from FIR–sub-mm–radio data usually do not include a rigorous analysis of the errors and the uncertainties in the calculations (Hughes et al. 1998; Blain 1999; Carilli & Yun 1999; Carilli & Yun 2000; Dunne, Clements & Eales 2000; Eales et al. 2000; Barger, Cowie & Richards 2000). The need to understand the accuracy with which existing and future sub-mm observations can provide redshifts for individual galaxies, motivated the development of Monte-Carlo simulations that take into account the imprecise knowledge of the luminosity function of sub-mm galaxies, the dispersion in the luminosity-dependent SEDs, absolute calibration and observational photometric errors (Aretxaga et al. 2001a, 2001b).

The goal of the Monte-Carlo simulations is to assign a degree of confidence (probability) to the photometric redshift of any individual sub-mm galaxy, and hence provide a robust statistical measure of the redshift distribution for the sub-mm population. In the case of *BLAST* (and also SPIRE), the power of this simple technique to derive redshifts arises from the unique ability of these experiments to conduct observations at $250\text{--}500\mu\text{m}$ that bracket the ubiquitous rest-frame FIR peak (at $\sim 60\text{--}150\mu\text{m}$) in the SEDs of high-redshift ($1 \leq z \leq 4$) galaxies undergoing a significant amount of star formation.

We have generated mock catalogues of galaxies between

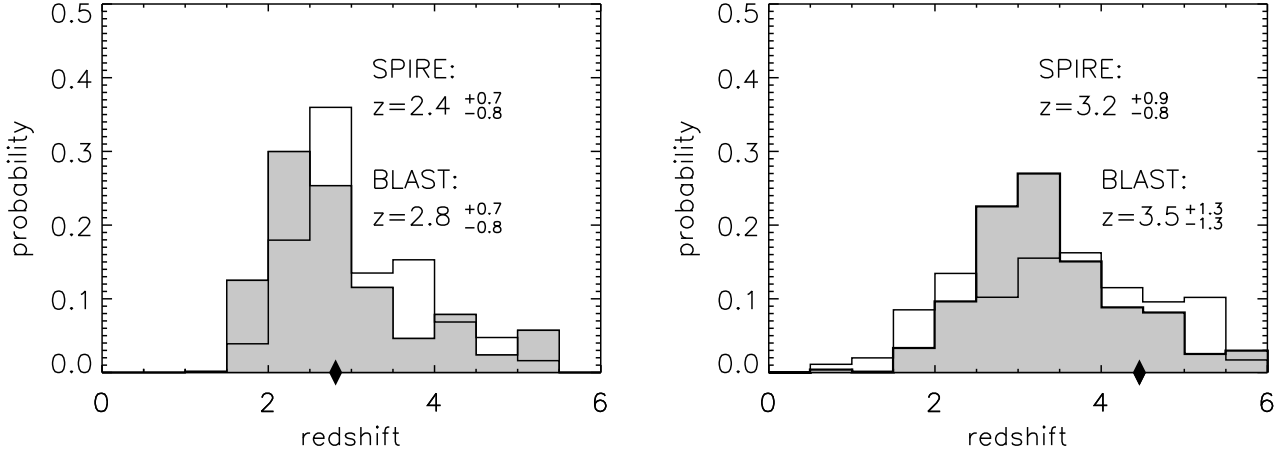


Figure 8. A comparison of the redshift probability distributions for two galaxies observed in a SPIRE survey, and a shallower *BLAST* survey (previously discussed in Fig.6). Symbols and labels are the same as in Fig.6. *Left panel*: $4 \times 10^{12} L_{\odot}$ galaxy at $z = 2.81$ detected simultaneously with 3 SPIRE filters (shaded histogram), compared with the *BLAST* redshift distribution (open histogram). *Right panel*: $4 \times 10^{12} L_{\odot}$ galaxy at $z = 4.46$ detected simultaneously in 2 SPIRE filters; at $350\mu\text{m}$ (11 mJy) and $500\mu\text{m}$ (20 mJy), compared with the distribution obtained from a single filter ($500\mu\text{m}$) detection with *BLAST*.

survey area (sq. deg)	1 σ depth	no. of pixels	no. of detected galaxies > 5 σ	no. of detected galaxies > 10 σ	no. of > 5 σ galaxies $z > 1$	no. of > 5 σ galaxies $z > 3$
1.0	5 mJy	18334	835	265	765	147
2.0	7 mJy	36668	1012	291	927	151
4.0	10 mJy	73336	1100	294	988	147
9.0	15 mJy	165006	1111	247	1023	129
36.0	30 mJy	660024	990	246	895	105

Table 1. Examples of the number of detected galaxies and their redshift distributions in alternative 50 hour $250\mu\text{m}$ *BLAST* surveys to be undertaken during a series of future long duration balloon flights in Antarctica.

$z = 0$ and $z \sim 6$. The adopted recipe, for a given wavelength and under the chosen cosmological model, is summarised:

(i) use a single representative SED to calculate the distribution of rest-frame FIR luminosities of galaxies, at all redshifts, from an evolving $60\mu\text{m}$ local luminosity function, $\phi[L, 0]$ (Saunders et al. 1990), that reproduces the observed sub-mm number counts. We adopt a model of pure luminosity evolution, $\phi[L, z] = \phi[L/L^*(z)]$, where

$$L^*(z) = \begin{cases} (1+z)^{3.2} L^*(0) & \text{for } z \leq 2 \\ 33.6 L^*(0) & \text{for } 2 < z \leq 6 \end{cases} \quad (1)$$

It has been verified that small differences in the evolutionary model still reproduce the source-counts (Fig.2);

(ii) randomly assign an SED from a library of 13 template starburst galaxies, ULIRGs and AGN (Fig.4) to each of the galaxies in the mock catalogue, and use this SED to calculate the intrinsic sub-mm colours. The most crucial assumption of the paper occurs at this point in the simulation. We assume no correlation between the shape of the SED and

luminosity (or redshift), and instead rely on the assumption that our library of template SEDs is representative of those that exist at high- z ;

(iii) add random noise (drawn from the distribution describing the measurement errors) and a constant absolute flux calibration error to the intrinsic fluxes to allow a more realistic assessment of the photometric redshift accuracy: 1 σ photometric errors of 5 and 2.5 mJy for the *BLAST* and Herschel/SPIRE observations respectively, and in both cases an absolute calibration error of 5%. The combined simulated images of extragalactic sources and cirrus, described earlier in §2.1, determine the depth of the surveys considered here, ensuring that galaxy confusion dominates. However this Monte-Carlo treatment of the photometric accuracy does not consider the contaminating effects of cirrus, clustering of galaxies, shot-noise or projection effects. These considerations are deferred to a future paper;

(iv) finally, extract flux-limited catalogues from a 1 sq. degree confusion-limited surveys at 250 , 350 and $500\mu\text{m}$

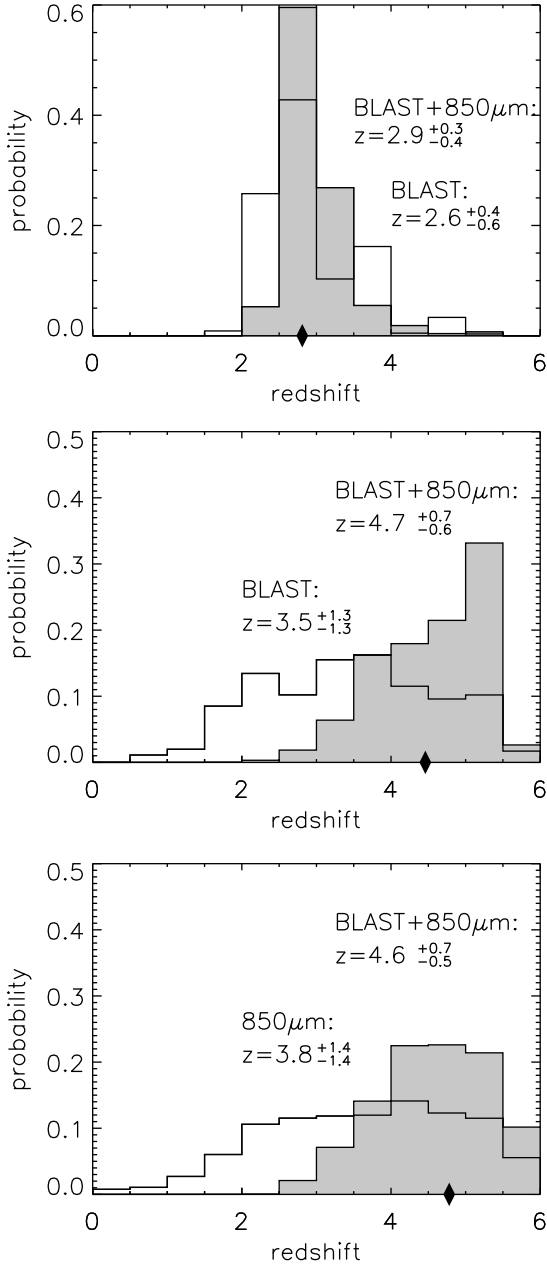


Figure 9. Redshift probability distributions demonstrating the advantages of follow-up observations that extend the sub-mm wavelength coverage. Symbols and labels are the same as in Fig.6. *Top panel:* $6 \times 10^{12} L_\odot$ galaxy at $z = 2.81$ detected by *BLAST* in all 3 filters (open histogram), previously discussed in Fig.6. The redshift estimate improves with follow-up observations at longer wavelengths. The shaded histogram illustrates the benefit of detecting the same galaxy at 850 μ m (8 mJy) in a shallow sub-mm survey ($\sigma_{850\mu\text{m}} = 2.5$ mJy), e.g. similar to the UK 8 mJy SCUBA survey (Scott et al. 2001); *Middle panel:* This example shows the $4 \times 10^{12} L_\odot$ galaxy at $z = 4.46$, initially detected by *BLAST* in only one filter (500 μ m), previously discussed in Fig.6 (open histogram). Again, the detection at 850 μ m (16 mJy) is sufficiently discriminating to constrain the distribution to higher redshifts (shaded histogram). *Bottom Panel:* $5 \times 10^{12} L_\odot$ galaxy at $= 4.78$ detected at 850 μ m (8 mJy) in a shallow SCUBA survey (open histogram). Despite the non-detection of this galaxy by *BLAST*, in all 3 filters (250, 350, 500 μ m), these shorter wavelength data can place an improved constraint on the redshift distribution (shaded histogram).

with $1\sigma = 5$ mJy and 2.5 mJy sensitivities, appropriate for *BLAST* and SPIRE observations.

An example of one of the possible combinations of sub-mm colours, for a catalogue of ~ 424 galaxies detected ($> 3\sigma$) simultaneously at 250, 350 and 500 μ m in a 1 sq. degree *BLAST* survey, is shown in Fig.5. As expected the dispersion in sub-mm colours is dominated by the observational errors and not by the differences between the shapes of the template SEDs. This is particularly true when the colour ratios are determined over a relatively small wavelength interval, as is the case for the 250, 350 and 500 μ m *BLAST* observations. However, as we extend the wavelength baseline over which colours are calculated then the effect of differences in the galaxy SEDs on the photometric colours becomes increasingly significant. An example of this important effect can be found with the inclusion of longer wavelength data to the *BLAST* observations (§2.3.3), or perhaps more extreme, with the combination of 850 μ m and 1.4GHz fluxes (Carilli & Yun 2000) which are separated in wavelength by a factor > 200 . Thus, in general, without an adequate treatment of observational errors and a representative set of reference SEDs, photometric redshifts will be estimated with an over-optimistic accuracy.

2.3 Sub-mm Photometric Redshifts

Sub-mm photometric redshifts can be determined by calculating the probability that the the colours (including errors) of an observed sub-mm galaxy are consistent with the colours of every galaxy (with a known redshift) in the mock catalogue. The final redshift probability distribution, $P(z)$, of any galaxy is then simply the sum of the individual probabilities from the entire catalogue, or explicitly

$$P(z) = a \sum_{i, \forall z_i} \Phi(\mathbf{c}_i - \mathbf{c}_0) , \quad (2)$$

where a is the normalization constant, such that $\int_0^{z_{\max}} P(z) dz = 1$ where $z_{\max} = 6$. The multi-variate Gaussian probability distribution, Φ , for k colours, is given by

$$\Phi(\mathbf{c}_i - \mathbf{c}_0) = (2\pi)^{-k/2} |\mathbf{A}^{-1}|^{1/2} \times \exp\left(-\frac{1}{2}(\mathbf{c}_i - \mathbf{c}_0)' \mathbf{A}^{-1} (\mathbf{c}_i - \mathbf{c}_0)\right) , \quad (3)$$

where \mathbf{c}_i is the colour vector of the i th mock galaxy, such that $z_i \in [z - dz, z + dz]$, and \mathbf{c}_0 is the colour vector of the test sub-mm galaxy, for which we want to derive its redshift distribution. \mathbf{A} is the covariance matrix of the colour distribution, of elements

$$A_{\alpha\beta} = \langle (\bar{c}_\alpha - c_\alpha)(\bar{c}_\beta - c_\beta) \rangle , \quad (4)$$

for two colours α, β . In the majority of the analysis performed for this paper, the non-diagonal elements of the covariance matrix are small. When more than two colours are considered, for simplicity, the above prescription can be substituted with standard χ^2 statistics.

In this analysis, we have adopted redshift bins of width 0.5 ($dz = 0.25$). The most probable redshift of the test sub-mm galaxy will be given by the mode of the discrete $P(z)$ distribution, estimated as the centroid of the Gaussian that

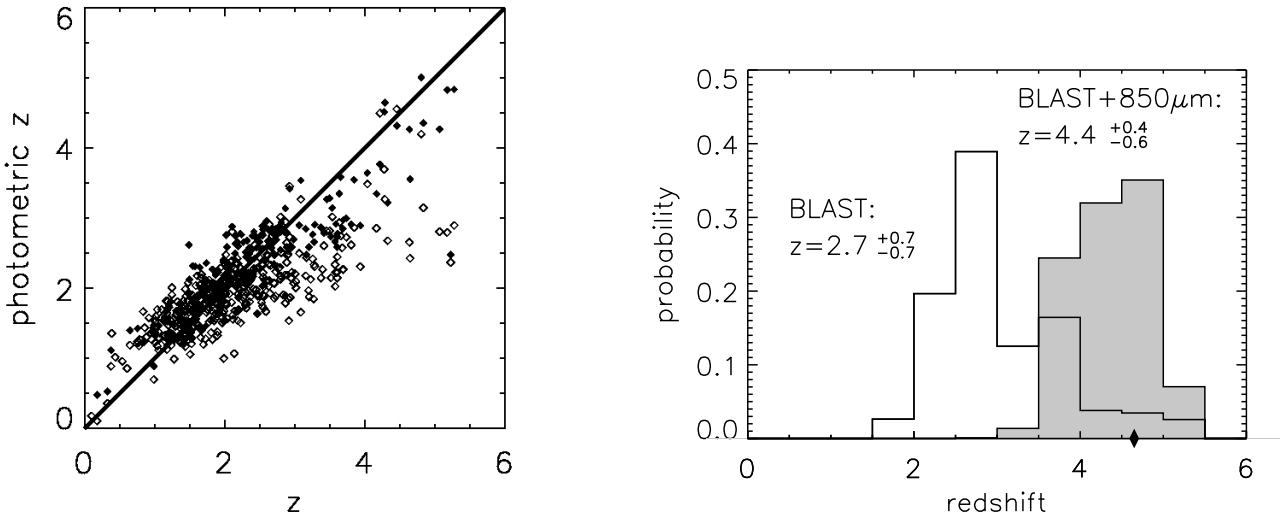


Figure 10. *Left panel.* Photometric redshift vs. true redshift relationship for 424 galaxies simultaneously detected at 250, 350 and 500 μm with *BLAST* in a 1 sq. deg survey. Open symbols show the relationship inferred using only *BLAST* data to derive the redshifts. Filled symbols show the relationships when the redshifts are estimated using colours based on *BLAST* and complementary 850 μm detections from a ground-based survey. The addition of 850 μm measurements significantly increases the accuracy at $z \geq 4$ since, at these redshifts, *BLAST* filters sample the rest-frame mid-IR to FIR ($\sim 35 - 100\mu\text{m}$). The longer wavelength data bracket the rest-frame FIR peak of the highest- z objects, which enhances the diagnostic power for the photometric technique discussed in this paper. *Right panel:* Example of the correction obtained for galaxies at $z > 4$ when 850 μm observations are included in the photometric redshift analysis. The redshift distributions for a $1 \times 10^{13} L_\odot$ galaxy at $z = 4.65$ with detections at 250 μm (18 mJy), 350 μm (29 mJy), 500 μm (27 mJy) and 850 μm (20 mJy) are shown as open (*BLAST* detections only) and shaded (*BLAST* and 850 μm detections) histograms. This correction, whilst significant, only applies to 4% of the entire sample detected in 3 bands.

best fits the 5 bins around the maximum of $P(z)$. The asymmetric error bars (z_- , z_+) correspond to 68% confidence levels such that $\int_{z_-}^{z_+} P(z) dz = 0.68$ and $(z_+ - z_-)$ is minimised.

2.3.1 *BLAST* colours

Fig.6 shows two examples of the redshift distributions for sub-mm galaxies detected by *BLAST* at different levels of significance in all 3 filters. A further example of the broader distribution derived for a higher- z galaxy detected only at 500 μm is also shown in Fig.6. The accuracy of the redshifts determined from *BLAST* data is described in more detail in §2.4, where we also compare the accuracy to those obtained from optical-IR colours and the 850 $\mu\text{m}/1.4\text{ GHz}$ spectral index. The dispersion in the sub-mm photometric redshifts derived from 3 *BLAST* bands is $\Delta z = \pm 0.6$ averaged over all redshifts in the range $0 < z < 6$.

2.3.2 *SPIRE* colours

An increase in the sensitivity of the sub-mm observations (with *SPIRE* for instance) naturally translates into an increased accuracy of the redshift distributions. Fig.7 shows the increased sample-size (at all redshifts) for the deeper *SPIRE* survey (compared to Fig.5). However the greater sensitivity of the *SPIRE* observations ($1\sigma = 2.5\text{ mJy}$) does not

significantly improve the accuracy of the redshift distributions, compared to those determined from detections in all 3 *BLAST* filters. The redshift uncertainties for these sources are due to a combination of the absolute calibration errors and the dispersion in the template SEDs. However *SPIRE* does provide a far greater redshift accuracy for the sources that *BLAST* detects in only one or two filters with low S/N (Fig.8). Thus, if the advantage of the larger aperture of *Herschel*, the reduced confusion limit and higher sensitivity of *SPIRE* is to be realised, then a clearer understanding of the SEDs of high- z galaxies is first required.

2.3.3 *BLAST + 850 μm colours*

A greater improvement in the accuracy of the sub-mm photometric redshifts can be achieved by following-up *BLAST* (or *SPIRE*) surveys with longer-wavelength survey data (e.g. ground-based 850 μm SCUBA data), or vice-versa. Fig.9 shows the result of simulations that combine *BLAST* and 850 μm observations. The SCUBA data include a photometric measurement error of 2.5 mJy, to compare with the shallow UK 8mJy SCUBA survey (Scott et al. 2001), and an absolute calibration error of 9%. The addition of a longer-wavelength datum to the colour information has two advantages. First, the inclusion of one more colour simply assists the ability to constrain the redshift. This is particularly important for galaxies detected only at 500 and/or 350 μm

(40% of the sources in the *BLAST* surveys), which lie at the highest redshifts. Second, at $z > 4$ the *BLAST* filters all begin to sample the short-wavelength (rest-frame mid-IR) side of the FIR peak. This 850 μm extension to the *BLAST* wavelength coverage (250–500 μm) ensures that there is still a long-wavelength datum that brackets the rest-frame FIR peak (at least until $z \sim 7$). A clear illustration of these benefits is shown in Fig.10 where high- z galaxies at $z > 4$, that had previously been confused with lower- z galaxies at $z = 2 - 3$ (using only data at 250–500 μm), are now symmetrically distributed about the $z = z_{\text{phot}}$ regression line over the entire range $0 < z < 6$, with an improved average error of $\Delta z \sim \pm 0.4$. This correction applies only to a small fraction (4%) of the galaxies detected in all 3 *BLAST* bands. This sub-mm method therefore continues to provide un-biased estimates of photometric redshifts for the most distant galaxies.

Given this benefit of including longer-wavelength data, the deepest *BLAST* surveys will be selected to overlap the largest (0.5 deg 2) southern surveys at dec = -15° of the JCMT at 850 μm and IRAM at 1.25 mm. The LMT will conduct southern hemisphere mm-surveys on scales of 10 deg 2 in 2005 down to a declination limit of -30° , providing even greater overlap with the *BLAST* surveys and, with the extended wavelength coverage (250 μm – 1.1 mm), providing accurate redshift constraints out $z \sim 8$.

The analysis described in this paper simultaneously makes use of all of the available multi-frequency data (unlike the simple one-colour vs. redshift treatments described elsewhere), and takes into account the measurement errors and uncertainties in the SEDs of the template galaxies used to extrapolate the rest-frame luminosities of the sub-mm galaxies from their observed data.

2.4 Comparison of Optical-IR, Sub-mm and Sub-mm–Radio Photometric Redshifts

The photometric redshifts of galaxies derived from sub-mm *BLAST* data (250, 350 and 500 μm), using the method described above, are compared with the true redshifts in our mock catalogues. We demonstrate that an average accuracy of $\Delta z(\text{submm}) \sim 0.6$ can be achieved over the range $0 < z < 6$, although, as Table 2 shows, the scatter increases significantly for $z > 3.5$ for the reasons described in §2.3. The photometric redshifts measured from the optical-IR SEDs of galaxies in the HDF (Fernández-Soto, Lanzetta, Yahil 1999; Rowan-Robinson 2001) have an accuracy that varies between $\Delta z(\text{opt}) \sim 0.1 - 0.6$ over the same redshift range. However we note that the optical galaxies described in this HDF analysis are obviously not drawn from the same population as the sub-mm galaxies. The accuracy of the optical photometric redshifts must be much poorer if the technique is applied to the optically-obsured SCUBA galaxies. The inclusion of longer wavelength data (*e.g.* 850 μm) to the *BLAST* data improves the photometric redshift accuracy to $\Delta z(\text{submm}) \sim 0.4$, and extends the redshift range over which we can measure reliable redshifts to $0 < z < 6$ (Fig.11 and Table 2). This means that, despite the greater wealth of data describing the optical-IR SEDs of galaxies and the number of available optical-IR bands, the sub-mm photometric redshifts of the sub-mm galaxy population can be

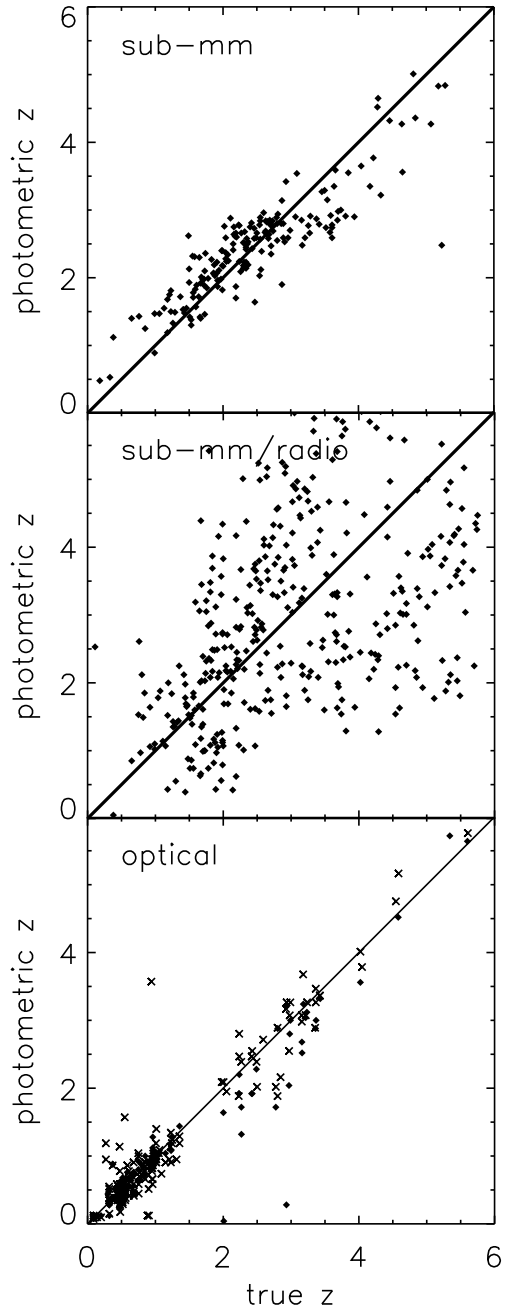


Figure 11. *Top panel:* Sub-mm photometric redshifts vs. true redshifts for 189 mock galaxies simultaneously detected at 250, 350, 500 and 850 μm in 1 sq. deg. The overall r.m.s. scatter in the sub-mm photometric redshifts, determined from the combined *BLAST* and SCUBA 850 μm data, is $\Delta z(\text{submm}) \sim 0.4$ in the redshift range $0 < z < 6$; *Middle panel:* Sub-mm–radio photometric redshifts vs. true redshifts for galaxies selected from the same catalogue as in the top panel, using $\alpha_{1.4}^{350}$, the 350–1.4 GHz spectral index described by Carilli & Yun (2000); *Bottom panel:* Optical–IR photometric redshifts vs. spectroscopic redshifts in the Hubble Deep Field - 108 galaxies (Fernández-Soto, Lanzetta, Yahil 1999 - diamonds), 156 galaxies (Rowan-Robinson 2001 - crosses). The optical–IR photometric redshifts, for galaxies at $z_{\text{true}} \geq 2$, show a dispersion of $\Delta z(\text{opt}) \sim 0.5$ (excluding the outlying sources).

redshift bin z	optical + IR	redshift accuracy Δz		
		BLAST	BLAST + 850 μ m	850 μ m + 1.4 GHz
0.5 – 1.5	0.1 (0.2)	0.3	0.5	0.7
1.5 – 2.5	0.5 (0.3)	0.3	0.3	1.2
2.5 – 3.5	0.5 (0.4)	0.7	0.3	1.4
3.5 – 4.5	0.5 (0.2)	1.1	0.7	2.1
4.5 – 5.5	0.3 (0.6)	2.1	0.6	2.5

Table 2. Comparison of the 1σ redshift accuracy, Δz , using different photometric colours in redshift bins between $0.5 < z < 5.5$: Column 2 - optical data (Fernandez-Soto et al. 1999, and Rowan-Robinson 2001 in parentheses); column 3 - sub-mm data from *BLAST* at 250, 350 and 500 μ m; Column 4 - extended sub-mm data from *BLAST* and additional 850 μ m observations; Column 5 - sub-mm (850 μ m, 350 GHz) and radio (1.4 GHz) data. Redshifts have been calculated from $\alpha_{1.4}^{350}$, defined as the spectral index between 350 and 1.4 GHz, using the formalism described by Carilli & Yun (2000). The redshifts in Cols. 3, 4 and 5 have been calculated for galaxies drawn from the same mock catalogue.

determined with a similar accuracy to the optical-IR photometric redshifts of optically-selected galaxies at $z > 1.5$.

The redshift accuracies determined from *BLAST* and *BLAST*+850 μ m data (cols. 3 and 4 in Table 2) are compared with those obtained from the identical data in our mock catalogues using the 350 GHz (850 μ m) to 1.4 GHz spectral index ($\alpha_{1.4}^{350}$) described by Carilli & Yun (2000). The simulations include a photometric error of 7 μ Jy, and absolute calibration error of 3% to compare with the deepest VLA surveys. As Figure 11 clearly illustrates, the photometric redshifts obtained with the sub-mm/radio method suffer a large scatter ($\Delta z(\alpha_{1.4}^{350}) > 1.5$), particularly at $z > 2$, where small differences in $\alpha_{1.4}^{350}$ result in large differences in the redshift estimates. The inability of the 850–1.4 GHz index to determine accurate redshifts at $z > 2$ has already been noted by Carilli & Yun (2000). At $z < 2.5$, photometric redshifts using $\alpha_{1.4}^{350}$ are still less accurate than those determined from the sub-mm (250–850 μ m) method described in this paper. This is due, in part, to the larger scatter of the SEDs at radio wavelengths (Figure 4). Naturally, any redshift estimated from a single colour index (e.g. $\alpha_{1.4}^{350}$) is also, in general, going to offer a less stringent constraint than the use of two or more colours.

2.5 Measuring the Star Formation History from Sub-mm Surveys

The measurement of redshift probability distributions for a large sample of sub-mm galaxies provides the information necessary to derive robust estimates of global properties of the population, such as the SFR history, even if the redshift and luminosity of individual galaxies are not known with a great degree of precision. The photometric redshift distribution of an individual galaxy allows the determination of its probable contribution to the total FIR luminosity density in a given redshift interval.

This calculation is performed via 100 Monte-Carlo samples drawn from the redshift probability distribution for each galaxy in the mock survey. The FIR luminosities of these galaxies are then derived from the fluxes in the mock catalogue and the new synthetic redshifts. The SED from the

template library that best represents the colours (including observational errors) of the whole population is used to calculate the necessary k-correction. This SED will in general be different from that assigned in the original catalogue. We then calculate the uncertainty in the k-correction, and therefore the error in the FIR luminosity, by randomly selecting any SED in the template library. Thus we remove any bias introduced into the reconstruction of the SFR through the choice of a single SED intended to represent the whole population of sub-mm galaxies. Finally, the star formation density is calculated from the mean of the Monte-Carlo FIR luminosities, assuming $SFR/M_{\odot}\text{yr}^{-1} = 2.0 \times 10^{-10} L_{\text{FIR}}/L_{\odot}$ (Hughes, Dunlop, Rawlings 1997).

A deep *BLAST* survey, combined with a wide-area shallow SCUBA survey ($S_{850\mu\text{m}} > 8$ mJy), can recover the SFR density due to galaxies with $L_{\text{FIR}} \geq 3 \times 10^{12} L_{\odot}$ at $0.5 \leq z \leq 5.5$ with an accuracy of $\sim 20\%$ (Fig.12). The completeness of the survey is $\sim 98\%$ above $3 \times 10^{12} L_{\odot}$ (Fig.12). The SFR density derived from the mock combined *BLAST* and SCUBA survey is consistent with the preliminary results from the UK 8 mJy SCUBA survey (Scott et al. 2001), and provides a good illustration of the advantage of being able to derive photometric redshifts for the entire survey sample over a large redshift range.

3 CONCLUSIONS

Monte-Carlo simulations of multi-wavelength (250–850 μ m) sub-mm surveys show that the majority of the scatter in the derived sub-mm colours will be due, in approximately equal parts, to the dispersion in the SEDs of galaxies in our library of templates, and the observational and calibration errors. Since we can control to some extent the quality of the experimental data, it is still the uncertainty in the observed (or model) SEDs of high- z starburst galaxies that will ultimately limit the accuracy of these photometric redshift predictions. Theoretical SEDs, based on radiative transfer models for high- z starburst galaxies (Efstathiou, Rowan-Robinson, Siebenmorgen 2000), can help in principle. However the low S/N, and restricted wavelength coverage of the available observational data for high- z starburst galaxies are consistent with such a broad range of theoretical models that they currently provide little discriminatory power in determining the most appropriate SEDs to use as templates. Consequently, one of the most straight-forward achievements of *BLAST*, but no less important, will be simply to provide an accurate empirical model of the temperature-sensitive SEDs for 1000’s of high- z galaxies at these critical short sub-mm wavelengths (250–500 μ m).

The product of the simulations of sub-mm surveys described in this paper is the ability to calculate the probability distribution for the redshift of any individual galaxy, taking into account observational errors and the uncertainty in the appropriate template SED, without the requirement to first identify the optical, IR or radio counterpart. These simulations demonstrate that the combination of balloon-borne (airborne or satellite) short-wavelength sub-mm data at 250–500 μ m, and longer-wavelength ground-based 850 μ m data, for a statistical sample of galaxies can provide the rest-frame FIR luminosity distribution, and hence the star formation history of the entire sub-mm population.

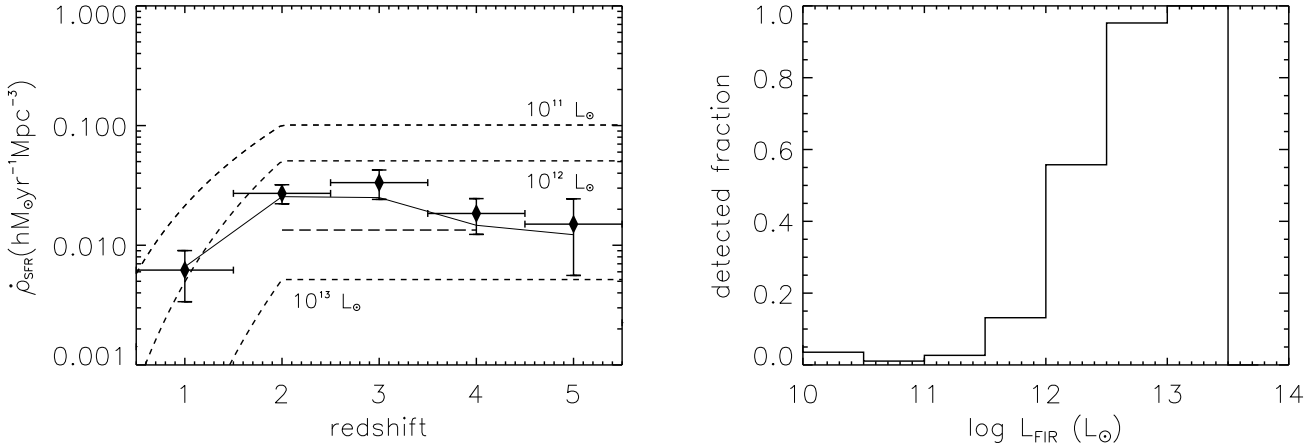


Figure 12. *Left panel:* Global star formation rate history of galaxies detected in at least 2 filters from a combined *BLAST* ($3\sigma = 15$ mJy) and wide-area SCUBA 850 μm survey ($3\sigma = 8$ mJy). Filled diamonds represent the recovered values of the SFR using the photometric redshift distributions. We compare these values with the true SFR included in the mock catalogue (shown as a solid line) before measurement errors are introduced. The 3σ error bars of the reconstructed SFR are dominated by the uncertainty of the SED that should be used to derive the 60 μm luminosities of the mock galaxies (which have intrinsically different SEDs), and not by the accuracy of the redshift determinations. The long-dashed horizontal line shows an estimate of the minimum SFR density for sub-mm galaxies that have been detected in the UK 8mJy SCUBA 850 μm survey (Scott et al. 2001), assuming that the SCUBA galaxies lie between $2 < z < 4$. The short-dashed curves represent the theoretical SFR due to galaxies of FIR luminosities $> 10^{11-13} L_\odot$ derived from the evolutionary model adopted in the simulations §2.2. *Right Panel:* Fraction of galaxies, per luminosity interval, detected at all redshifts in the mock combined *BLAST* and wide-area SCUBA survey. The completeness of the survey is $\sim 98\%$ for galaxies $> 3 \times 10^{12} L_\odot$.

The precision of redshift estimates determined from short-wavelength sub-mm observations (250–500 μm) is encouraging, with a 1σ dispersion of $\Delta z(\text{submm}) = 0.4 - 0.6$ (depending on the availability of longer-wavelength ground-based data, $\lambda \geq 850\mu\text{m}$) over the range $0 < z < 6$. This sub-mm precision is comparable to the accuracy of the optical-IR photometric estimates of redshift, $\Delta z(\text{opt}) \sim 0.5$ at $z > 2$, and significantly better than those provided by the 850 $\mu\text{m}/1.4$ GHz spectral index. An important consequence of these sub-mm redshift constraints is the ability to measure the star-formation of luminous sub-mm galaxies ($L_{\text{FIR}} > 3 \times 10^{12} L_\odot$) with an unprecedented error of $\sim 20\%$.

The advantage of having a constrained redshift probability distribution for individual sub-mm galaxies, without optical, IR or radio (continuum) counterparts, is that we can now determine the likelihood that a redshifted rotational CO transition-line falls into the frequency range of any particular spectral-line receiver on the next generation of large mm-cm telescopes (*e.g.* 100-m GBT, 50-m LMT). The opportunities to conduct mm-wavelength spectroscopic follow-up observations that will provide definitive molecular-line redshifts, and dynamical-mass estimates of sub-mm galaxies, are discussed further in Paper II (Aretxaga et al. 2001b).

The combination of short-wavelength sub-mm data from *BLAST*, SPIRE or other facilities, and large single-dish millimetre wavelength telescopes provides a powerful combination to break the *redshift deadlock* that hinders our

ability to understand the evolution and nature of the sub-mm starburst galaxy population.

4 ACKNOWLEDGMENTS

This work has been funded by CONACYT grants 32180-E and 32143-E. The development of *BLAST* is supported in part by NASA grant NAG5-92291. DHH, IA, and ELC would like to thank Mark Devlin and the Physics & Astronomy Dept. at Univ. of Pennsylvania, Philadelphia for their financial support and hospitality in June 2001 during which time part of this work was carried out.

REFERENCES

- Aretxaga I., Hughes D.H., Chapin E., Gaztañaga E., 2001a, in M. de Petris & M. Gervasi, *Experimental Cosmology at Millimetre Wavelengths*, AIP, Cervino, in press, astro-ph/0111508
- Aretxaga I., Hughes D.H., Chapin E., Gaztañaga E., Dunlop J.S., 2001b, in preparation (paper II)
- Barger A.J., et al., 1998, *Nature*, 394, 248
- Barger A.J., Cowie, L.L., Richards, E.A., 2000, *A.J.*, 119, 2092
- Baugh C.M., Cole S., Frenk C.S., 1996, *MNRAS*, 283, 1361
- Bertoldi F., et al., 2000, in D.J. Wilner et al., *Cold Gas and Dust at High Redshift*, Highlights of Astronomy 12, in press, astro-ph/0010553
- Blain A.W., 1999, *MNRAS*, 309, 955

Blain A.W., Longair M.S., 1993, MNRAS, 264, 509

Borys C., Chapman S.C., Halpern M., Scott D., 2001, submitted to MNRAS, astro-ph/0107515

Carilli C.L., Yun M.S., 1999, Ap.J., 513, L13

Carilli C.L., Yun M.S., 2000, Ap.J., 530, 618

Chapin E., Hughes D.H., Kelly B.D., Holland W.S., 2001, in M. de Petris & M. Gervasi, *Experimental Cosmology at Millimetre Wavelengths*, AIP, Cervino, in press, astro-ph/0109330

Chapman S.C. et al., 2000, MNRAS, 319, 318

Condon J.J., 1974, Ap.J., 188, 279

Désert F.X., Boulanger F., Puget J.L., 1990, A&A, 237, 215

Devlin M. et al., 2001, in J.Lowenthal & D.H.Hughes, *Deep Millimetre Surveys: Implications for Galaxy Formation and Evolution* World Scientific, in press, astro-ph/0012327

Downes D., et al., 1999, A&A, 347, 809

Dunne L., Clements D.L., Eales S.A., 2000, MNRAS, 319, 813

Eales S.A., et al., 1999, Ap.J., 515, 518

Eales S.A., et al., 2000, A.J., 120, 2244

Efstathiou A., Rowan-Robinson M., Siebenmorgen R., 2000, MNRAS, 313, 734

Fernández-Soto A., Lanzetta K., Yahil A., 1999, Ap.J., 513, 34

Fixsen D.J., et al., 1998, Ap.J., 508, 123

Fox M.J., et al., 2001, MNRAS, in press, astro-ph/0107585

Frayer D.T., et al., 1998, Ap.J. Lett., 506, L7

Frayer D.T., et al., 2000, A.J., 120, 1668

Gautier T.N., Boulanger F., Pérault M., Puget J.L., 1992, A.J., 103, 1313

Gaztañaga E., Hughes D.H., 2001, in J.Lowenthal & D.H.Hughes, *Deep Millimetre Surveys: Implications for Galaxy Formation and Evolution*, World Scientific, in press, astro-ph/0103127

Gaztañaga E., Hughes D.H., Artxaga I., Chapin E., 2002, in preparation (paper III)

Gear W.K., et al., 2000, MNRAS, 316, 51

Glenn J., et al., 1998, in T.G. Phillips, *Advanced Technology MMW, Radio, and Terahertz Telescopes*, Proceedings of SPIE Vol. 3357

Hauser M.G., et al. 1998, A.J., 115, 1418

Holland W.S., et al., 1999, MNRAS, 303, 659

Hughes D.H., 2000, in A.Mazure, O. Le Févre, V. Le Brun Clustering at High Redshift, ASP Conf. 200, 81, astro-ph/0003414

Hughes D.H., Dunlop J.S., Rawlings S., 1997, MNRAS, 289, 766

Hughes D.H., et al., 1998, Nature, 394, 241

Hughes D.H., Gaztañaga, E., 2000, in F.Favata & A.Kass, *Star formation from the Small to the Large Scale*, ESA SP-445, p.29, astro-ph/0004002

Hunter T.R., Benford D.J., Serabyn E., 1996, PASP, 108, 1042

Ivison R.J., et al., 2000, MNRAS, 315, 209

Ivison R.I., et al., 2001, MNRAS, 298, 583

Kauffmann, G., White, S.D.M., Guiderdoni, B., 1993, MNRAS, 264, 201

Knudsen K.K., van der Werf P.P., Jaffe W., 2001 in J.Lowenthal & D.H.Hughes, *Deep Millimetre Surveys: Implications for Galaxy Formation and Evolution*, World Scientific, in press, astro-ph/0009024

Kreysa E. et al., 1998, in T.G. Phillips, *Advanced Technology MMW, Radio, and Terahertz Telescopes*, Proceedings of SPIE Vol. 3357

Lagache G., Puget J.L., 2000, A&A, 355, L17

Lilly S.J., et al., 1999, Ap.J., 518, 441

Lutz D., et al., 2001, A&A, 378, 70

Madau P., et al., 1996, MNRAS, 293, 1388

Peacock J.A., et al. 2000, MNRAS, 318, 535

Puget J.-L., et al. 1996, A&A, 308, L5

Richards E.A., 1999, Ap.J., 513, L9

Rowan-Robinson M., 2001, Ap.J., submitted, <http://astro.ic.ac.uk/~mrr/photz/photzapj.ps>

Sanders D.B., Mirabel I.F., 1996, ARA&A, 34, 749

Saunders W. et al., 1990, MNRAS, 242, 318

Schlegel D.J., Finkbiener D.P., Davis, M., 1998, Ap.J., 500, 525

Scott D., et al., 2000, A&A, 357, L5

Scott S., et al., 2001, MNRAS, in press, astro-ph/0107446

Smail I., et al., 1997, MNRAS, 490, L5

Smail I., Ivison R.J., Blain A.W., Kneib J.-P., 1998, 507, L21

Smail I., et al., 1999, MNRAS, 308, 1061

Smail I., et al., 2000, Ap.J., 528, 612

Somerville R.S., Primack J.R., Faber S.M., 2001, MNRAS, 320, 504

Steidel C.C., et al., 1996, Ap.J, 462, L17